Journal of Alloys and Compounds 685 (2016) 724–732

Contents lists available at ScienceDirect

Journal of Alloys and Compounds

journal homepage: http://www.elsevier.com/locate/jalcom

Experimental investigation of Mg-Zn-Al metal alloys for latent heat storage application

Elena Risueño [a], Stefania Doppiu [a], Javier Rodríguez-Aseguinolaza [a], Pablo Blanco [a], Antoni Gil [a], Manuel Tello [b], Abdessamad Faik [a, *], Bruno D'Aguanno [a]

[a] CIC Energigune, Albert Einstein 48, 01510 Miñano, Álava, Spain
[b] Depto. Física de la Materia Condensada, Facultad de Ciencia y Tecnología, Universidad del País Vasco, Apdo. 644, 48080 Bilbao, Spain

ARTICLE INFO

Article history:
Received 15 March 2016
Received in revised form
3 June 2016
Accepted 21 June 2016
Available online 23 June 2016

Keywords:
Thermal energy storage
Metallic materials
Mg-Zn-Al alloy
Phase change material
Latent heat storage
High thermal conductivity

ABSTRACT

In this paper the use of metallic alloys is proposed as high thermal conductivity phase change materials (PCM) for thermal energy storage (TES). The high thermal conductivity of the proposed metallic PCMs is around two orders of magnitude higher than the one of materials (molten salt) commonly used on TES applications. This would present great benefits in several applications frames from the concentrated solar power (CSP) to industrial heat recovery. In this work, three different alloys, with different Al content, have been selected from the Mg-rich corner of Mg-Zn-Al ternary phase diagram with general formulas $Mg_{71}Zn_{28.9}Al_{0.1}$, $Mg_{70}Zn_{24.9}Al_{5.1}$ and $Mg_{70}Zn_{24.4}Al_{5.6}$. The first and third materials correspond to quasi-peritectic compositions and the second material corresponds to a eutectic composition. The eutectic compositions, in general, are considered more suitable as PCMs for TES application due to their long-term stability under charging discharging cycles. The two quasi-peritectic compositions have been selected to investigate the influence of the chemical composition changes on the thermophysical properties and consequently to study their potentiality regarding the energy storage density factor.

In this work, a complete structural and thermophysical characterization of the selected metal alloys has been carried out in order to obtain the driving parameters for latent heat storage applications. In general, the obtained results confirm the suitability of the investigated metals alloys as high thermal conductivity phase change materials for latent heat energy storage.

1. Introduction

Thermal energy storage (TES) systems have become a key issue on an efficient management of the available energetic sources [1]. Their implementation in different applications, such as concentrated solar power (CSP) plants [2,3] and industrial waste heat and industrial processes [4–6], has shown a very high potential in order to increase the global efficiency of the involved processes and to reduce the energy consumption. Thermal energy storage (TES) technologies are predominantly based on molten salt mixtures as sensible heat storage material [7–9]. This approach has extensively been used in many concentrated solar power (CSP) plants implementing the two-tank molten salt solution. As a consequence, this storage system has become a developed and mature technology. Currently, the latent heat storage (LHS) has attracted the attention of the scientific and technologic community [10–12]. Several advantages are associated to this storage method, such as, the isothermal operation behaviour and the large storage capacity based on the high energy storage density. Up to now, in high temperature range, different phase change materials (PCM), like inorganic salts, have been proposed and investigated in different applications [13,14]. Recently, the sodium nitrate ($NaNO_3$), with melting temperature 306 °C, thermal conductivity 0.6 W/m K and latent heat 175 kJ/kg, was successfully tested in 1 MW test facility for direct steam generation application [15]. However, the currently proposed PCMs present several shortcomings like their low thermal conductivity which need to be overcome in the next generation of TES technologies. This leads to a poor heat transfer in the material and to the need of using sophisticated heat exchanger devices in order to reach an acceptable heat transfer between the storage media and the heat transfer fluid [13,16,17].

In this work, the use of metallic alloys as LHS materials is proposed as an innovative solution addressing the low thermal conductivity limitation of the convectional PCMs. Among the

* Corresponding author.
E-mail address: afaik@cicenergigune.com (A. Faik).

http://dx.doi.org/10.1016/j.jallcom.2016.06.222
0925-8388/

advantages of these materials, derived from their high thermal conductivity, are their fast thermal response and the consequent high operation power level. The high thermal conductivity of these materials could not only represent a breakthrough concept regarding current storage technologies but also to protect some components, as receivers, against thermal shocks and to reduce the impact of solar fluctuations and received radiation transients. Moreover, these materials present very high decomposition temperatures which make them very important for new generation CSP plants where high operation temperature above 650 °C is predicted. Although several research groups have suggested and investigated the suitability of metals as storage materials [18–25], a deep effort is still needed at all levels, from the basic materials science to the final application development in order to develop a satisfactory solution.

In this scope, recent investigations in our laboratories have identified the $Mg_{72}Zn_{28}$ binary eutectic alloy as an appropriate LHS material [26,27]. The selection of this binary eutectic composition as potential PCM was performed due to its melting temperature in the operational temperature range of CSP plants, as well as, due to high fusion entropies, availability and low cost of Mg and Zn metals [18,19]. In these works, it has been demonstrated the main advantages of this material and its suitability as PCM for thermal energy storage applications due to its good thermophysical properties. One of the drawbacks regarding the material point of view is its sensitivity to the melt-cooling rate. Two different phase compositions are obtained: from one hand, the expected phases $Mg_{21}Zn_{25}$ and α-Mg are achieved with controlled cooling rate of 0.1 °C/min. From the other hand, the metastable compositions $Mg_{51}Zn_{20}$ and α-Mg are established with no-controlled cooling rate (5–10 °C/min). A high influence of the metastable behaviour of the $Mg_{72}Zn_{28}$ alloy on some thermophysical properties was observed. As an example, the experimental values of the thermal diffusivity obtained for the metastable phase are 40% much lower than the ones obtained for the stable phase in temperature range of 50–250 °C. In the present work, in order to overcome the meta-stability nature of the studied binary alloy and to identify new metal alloys candidates, the $Mg_{70}Zn_{24.9}Al_{5.1}$ ternary eutectic alloy, with close composition and similar melting temperature to the mentioned $Mg_{72}Zn_{28}$, has been selected, where the Al metal selection was also performed according to its high fusion entropy, availability and low cost. In addition, two quasi-peritectic alloys, $Mg_{71}Zn_{28.9}Al_{0.1}$ and $Mg_{70}Zn_{24.4}Al_{5.6}$, close to the selected ternary composition, have also been studied. The main motivations of this experimental work are to investigate the behaviour of different materials from the Mg-Zn-Al ternary system and to study the possible influence of the composition modifications on the structural stability of the materials and, consequently, on their driving thermophysical properties for the thermal energy storage applications.

The three selected materials are located in the Mg-rich corner of the Mg-Zn-Al system displayed in Fig. 1 [28]. Table 1 summarizes the general formula, atomic and weight compositions and the theoretical melting temperature of the investigated alloys. The $Mg_{71}Zn_{28.9}Al_{0.1}$, $Mg_{70}Zn_{24.9}Al_{5.1}$ and $Mg_{70}Zn_{24.4}Al_{5.6}$ ternary metal alloys have been synthesized and an exhaustive structural and thermophysical characterization has been conducted. The obtained results are compared to the ones of the eutectic binary composition in order to highlight their suitability as PCMs for thermal energy storage application.

2. Materials and methods

2.1. Material synthesis

Total amounts of about 60 mg of the selected alloys, $Mg_{71}Zn_{28.9}Al_{0.1}$, $Mg_{70}Zn_{24.9}Al_{5.1}$ and $Mg_{70}Zn_{24.4}Al_{5.6}$, were prepared by the stoichiometric proportion of the primary metals (purity higher than 99.99%), and then placed into an alumina crucible. To avoid the possible oxidation during the synthesis process the alumina crucibles were introduced inside small stainless steel reactors and closed hermetically in a glove box under argon inert atmosphere. The synthesis process was performed in a muffle furnace at 500 °C (heating rate of 10 °C/min) and maintained for 6 h. During the synthesis process an external mechanical movement was applied every 30 min in order to ensure the homogeneity of the synthetized alloy. Two different cooling rates of 10 °C/min and 0.1 °C/min were applied to study the effect of this parameter on obtained material microstructures. After the solidification, the alloy samples were mechanized in order to obtain the appropriate shape and size to subsequent characterization. Finally, in order to relax the stresses due to machining process, a thermal treatment below the melting temperature, at 300 °C, during 24 h was carried out. The correct composition and the homogeneity of the investigated alloys were confirmed by inductively coupled plasma (ICP – Ultima 2 Horiba) by analysing different parts of the prepared samples.

2.2. Characterization methods

2.2.1. X-ray powder diffractions (XRD) and scanning electron microscopy (SEM)

In order to identify the present phases in the alloys and to calculate their lattice parameters, X-ray powder diffraction analysis (XRD) was performed by means of a Bruker D8 Advance Diffractometer in Bragg-Brentano geometry (θ–θ) using $CuK_{\alpha 1,2}$ radiation. The data were collected between 5° and 80° in 2θ with a step size of 0.02° and 8 s per step. The treatment of the diffractograms was performed using the WinPlotr/FullProf package [29,30].

Scanning electron microscopy (SEM) investigations were performed using a Quanta FEG 250 microscope. Smooth surfaces of specimens were prepared by using SiC papers and diamond pastes down to 1 μm grain size. The samples were imaged in high vacuum mode at 30 kV using back scattered electron detector (BSED). The microscope is equipped with an Apollo 10 SSD energy-dispersive X-ray spectrometer (EDX) for elemental analysis.

2.2.2. Differential scanning calorimetry (DSC)

Differential scanning calorimetry (DSC) measurements were performed by using a TA Q2000 calorimeter to determine the melting/solidification temperatures, latent heat and specific heat of the studied metallic alloys. For melting and solidification temperatures and enthalpies determination, around 50 mg of the samples using alumina sample holders were measured. In order to check the repeatability of the results three cycles between 200 °C and 450 °C with heating and cooling rates of 10 °C/min and under argon flow of 100 ml/min have been carried out. The experimental error for the temperature and enthalpy are ±0.01 °C and ±0.1%, respectively.

The specific heat of the alloys has been measured by modulated quasi-isothermal DSC technique [26,31]. The selected experimental parameters are: 1 h for the modulation time, ±1 °C for the temperature amplitude and 120 s for the modulation period. The measurement of the specific heat was limited up to 200 °C in order to avoid possible corrosion mechanisms between the alloy and the aluminium crucibles in the liquid state. Under these experimental conditions, the experimental error of these measurements is lower than ±3%.

2.2.3. Thermal diffusivity by laser flash apparatus (LFA)

The thermal diffusivity of the alloys was determined by using a laser flash apparatus (LFA 457, Netsch). Three cycles from 50 °C to 400 °C were carried out. The measurements were performed each 50 °C in the solid phase and each 20 °C in the liquid phase. Disk shaped samples of 10 mm of diameter and 1.5 mm of thickness with

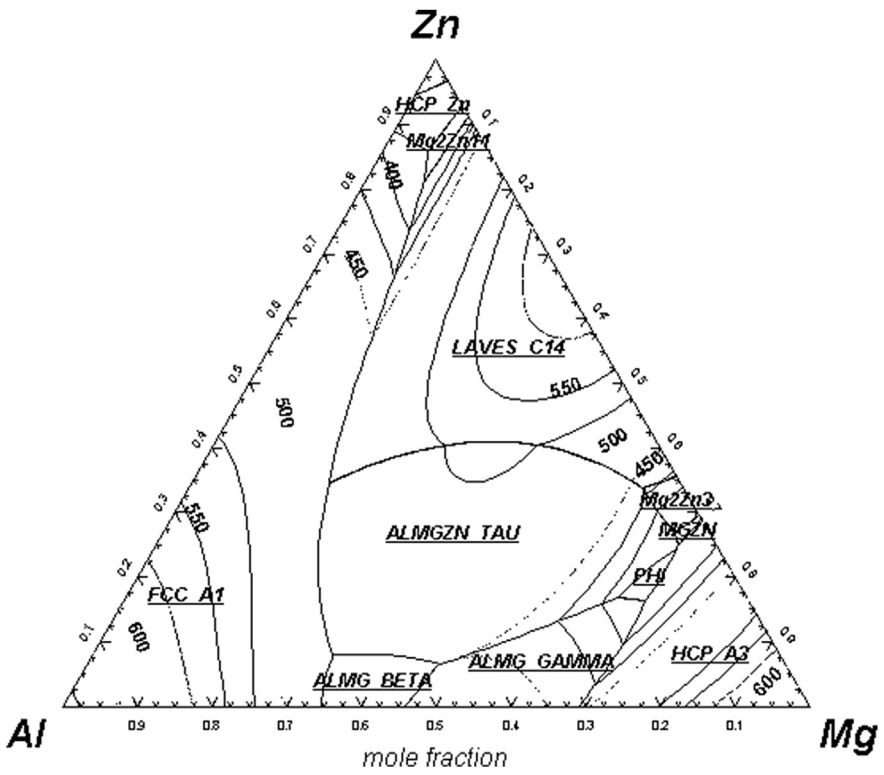

Fig. 1. Zn-Mg-Al liquidus projection [50].

graphite surface coating were measured under argon flow (50 ml/min). The estimated experimental error is lower than 5% [32,33]. The thermal conductivity was indirectly calculated using the equation: (1) $\lambda = \alpha \cdot \rho \cdot C_p$, where,$\lambda$ is the thermal conductivity (W/m K), α is the thermal diffusivity (mm^2/s), ρ is the density (kg/m^3) and C_p is the specific heat (J/g K).

3. Results and discussion

3.1. Structural analysis

Fig. 2 shows the X-ray diffractograms of $Mg_{71}Zn_{28.9}Al_{0.1}$, $Mg_{70}Zn_{24.9}Al_{5.1}$ and $Mg_{70}Zn_{24.4}Al_{5.6}$ alloys synthesized using a cooling rate of 10 °C/min. The results of the refinements show the presence of two phases in different proportions. The first one is an isostructural composition of the trigonal $Mg_{21}Zn_{25}$ intermetallic phase [34], and the second one is an isostructural composition of the hexagonal Mg phase [35]. According Mg-Zn-Al phase diagram [36], $Mg_{70}Zn_{24.9}Al_{5.1}$ and $Mg_{70}Zn_{24.4}Al_{5.6}$ alloys should present the cubic $Mg_{32}(Al,Zn)_{49}$ intermetallic compound as a third phase [37–39]. Ren et al. [40] suggested that $Mg_{32}(Al,Zn)_{49}$ is a metastable phase and its presence depends on the preparation conditions. Therefore, in order to study the effect of the cooling rate on the phases formation other materials have been prepared under slow cooling rate of 0.1 °C/min. The analysis of the diffractograms shows the presence of the same phases established under the previous cooling rate of 10 °C/min. From the one hand, this results shows that the $Mg_{32}(Al,Zn)_{49}$ has not been established under various cooling rates which is aligned with the result in Ref. [40]. From the other hand, this analysis demonstrates the stable behaviour of these ternary alloys independently of the applied cooling rates which is different to the metastable behaviour obtained for the $Mg_{72}Zn_{28}$ binary eutectic alloy where a random formation of two intermetallic phases (stable and metastable) was obtained [27]. The addition of Al metal (even a small amount of 0.1 at.%) to the Mg-Zn binary system leads to stabilise the system forming stable $Mg_{21}Zn_{25}$ intermetallic phase and Mg solid solution at room temperature.

Table 1
The compositions in atomic and weight portions, and the theoretical melting temperatures of $Mg_{71}Zn_{28.9}Al_{0.1}$, $Mg_{70}Zn_{24.9}Al_{5.1}$ and $Mg_{70}Zn_{24.4}Al_{5.6}$ alloys.

Alloy	Atomic percentage (%)			Weight percentage (%)			T_m (theoretical) (°C)	Ref.
	Mg	Zn	Al	Mg	Zn	Al		
$Mg_{71}Zn_{28.9}Al_{0.1}$	71	28.9	0.1	47.7	52.2	0.1	340.48	[28]
$Mg_{70}Zn_{24.9}Al_{5.1}$	70	24.9	5.1	49	47.1	3.9	338.36	[28]
$Mg_{70}Zn_{24.4}Al_{5.6}$	70	24.4	5.7	49.4	46.2	4.4	340.07	[28]

Table 2 shows the lattice parameters of the $Mg_{21}Zn_{25}$ and Mg isostructural phases obtained from the refinements in comparison to the lattice parameters of the pure phases obtained from ICSD database [34,35]. The refined lattice parameters are different to the ones of the pure $Mg_{21}Zn_{25}$ and Mg phases and these variations are related to the Zn and Al solubility in both structures.

In the case of $Mg_{71}Zn_{28.9}Al_{0.1}$ alloy, the calculated lattice parameters of both phases, $Mg_{21}Zn_{25}$ and Mg, are smaller than the ones of the pure reference phases. Considering the atomic radius of Mg (1.60 Å), Zn (1.42 Å) and Al (1.43 Å), the decrease of the lattice parameters indicates the substitution of the Mg atoms in both isostructural phases by the Zn and Al atoms which have smaller atomic radius.

In the case of $Mg_{70}Zn_{24.9}Al_{5.1}$ and $Mg_{70}Zn_{24.4}Al_{5.6}$ alloys two different effects in the lattice parameters are observed. As in $Mg_{71}Zn_{28.9}Al_{0.1}$ alloy, the lattice parameters of Mg solid solution decrease with the addition of Al due to the substitution of Mg by smaller Zn and Al atoms. However, the $Mg_{21}Zn_{25}$ phase lattice parameters increase with the addition of Al. This result suggests that the Al, present in these alloys, could be contained in the $Mg_{21}Zn_{25}$ intermetallic phase deforming its cell unit.

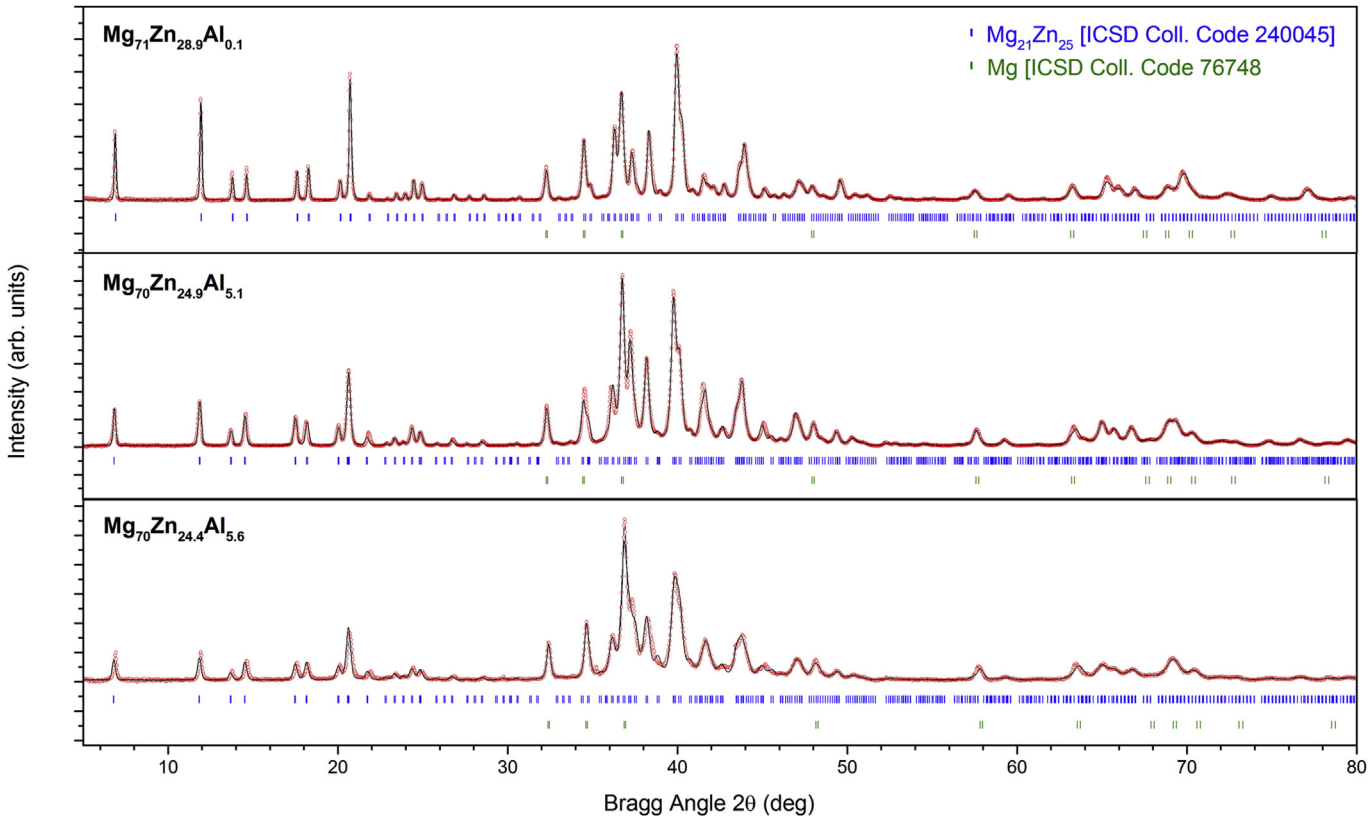

Fig. 2. Experimental (–) and calculated (oo) X-ray diffraction patterns for the refinements of $Mg_{71}Zn_{28.9}Al_{0.1}$, $Mg_{70}Zn_{24.9}Al_{5.1}$ and $Mg_{70}Zn_{24.4}Al_{5.6}$ alloy samples. The bars in the lower part of the graphics represent the Bragg peak positions that correspond to Mg (bottom) and $Mg_{21}Zn_{25}$ (top) isotropic phases.

To confirm the results observed by XRD measurements, scanning electron microscopy (SEM) experiments were performed. The images of three alloys are shown in Fig. 3 where each row of images corresponds to an alloy composition. In general, the observed structures by SEM confirm the eutectic and quasi-peritectic nature of the investigated alloys [41–43]. It can be observed that the crystal size of the phases increases with higher Al content in the material. However, in the case of the $Mg_{71}Zn_{28.9}Al_{0.1}$ alloy (Fig. 3 a, b and c), the small amount of the Al which actuates as an impurity, increases the number of germination nucleus. As a consequence, the crystal size is smaller and the structure is more refined. In the first column of Fig. 3, images at low magnification of the three samples cooled at 10 °C/min confirm the homogeneity of the prepared samples. Finally, in the second and third columns, images at high magnification of the samples cooled at 10 °C/min and 0.1 °C/min demonstrate that the decreasing of the cooling rate leads to larger crystal sizes.

Table 2
The refined lattice parameters of the $Mg_{21}Zn_{25}$ and Mg isotopic phases obtained from the refinements of the X-ray diffractograms of $Mg_{71}Zn_{28.9}Al_{0.1}$, $Mg_{70}Zn_{24.9}Al_{5.1}$ and $Mg_{70}Zn_{24.4}Al_{5.6}$ alloys. The lattice parameters of the pure phases are given for comparison.

Alloy	Mg lattice parameters(Å)			$Mg_{21}Zn_{25}$ lattice parameters (Å)		
	a(Å)	c(Å)	V(Å^3)	a(Å)	c(Å)	V(Å^3)
Mg	3.2093	5.2103	46.47	–	–	–
$Mg_{21}Zn_{25}$	–	–	–	25.7758	8.7624	5041.72
$Mg_{71}Zn_{28.9}Al_{0.1}$	3.2014	5.2004	46.16	25.7092	8.7281	4996.03
$Mg_{70}Zn_{24.9}Al_{5.1}$	3.1972	5.1901	45.95	25.8318	8.7296	5044.70
$Mg_{70}Zn_{24.4}Al_{5.6}$	3.1948	5.1909	45.90	25.8770	8.7302	5061.77

Additionally, the images provide a strong experimental confirmation of the existence of only two phases after the solidification processes. The black coloured microstructures correspond to the Mg isostructural phase and the white coloured ones to the $Mg_{21}Zn_{25}$ isostructural phase. An exhaustive microstructural inspection of the sample surfaces also confirms the absence of the cubic $Mg_{32}(Al,Zn)_{49}$ intermetallic phase in $Mg_{70}Zn_{24.9}Al_{5.1}$ and $Mg_{70}Zn_{24.4}Al_{5.6}$ alloys.

In order to determine the experimental compositions of the intermetallic phases present in each alloy EDX analysis was performed. Table 3 summarizes the observed phase compositions and their proportions compared to the theoretical ones obtained from the ternary phase diagram at room temperature [35]. Regarding the Mg isotopic phase compositions, it can be observed that Mg is substituted by Zn and Al. Moreover, it can be noted that increasing the Al proportion in the alloys, the Zn solubility in Mg phase also increases. It can also be remarked that the increasing of the Al proportion in the alloy leads to an increase of the Zn solubility in the composition of Mg phase, as Ren et al. observed in Ref. [44]. For the case of the experimental $Mg_{21}Zn_{25}$ isostructural phase composition of, around 8 at.% and 10 at.% Al solution have been found in $Mg_{70}Zn_{24.9}Al_{5.1}$ and $Mg_{70}Zn_{24.4}Al_{5.6}$ alloys, respectively. The Mg-Zn-Al phase diagram at room temperature indicates a maximum Al solubility around 2.5 at.% in $Mg_{21}Zn_{25}$ phase [36]. This discrepancy between experimental and theoretical values might be related to the absence of the $Mg_{32}(Al,Zn)_{49}$ phase in these alloys. As a consequence, the Al amount associated to the ternary phase was dissolved mainly in the $Mg_{21}Zn_{25}$ phase. Another consequence, of this anomalous Al distribution in this intermetallic phase, is the increase of the lattice parameter values, as indicated by the experimental XRD analysis. So, the extension of the Al solubility in

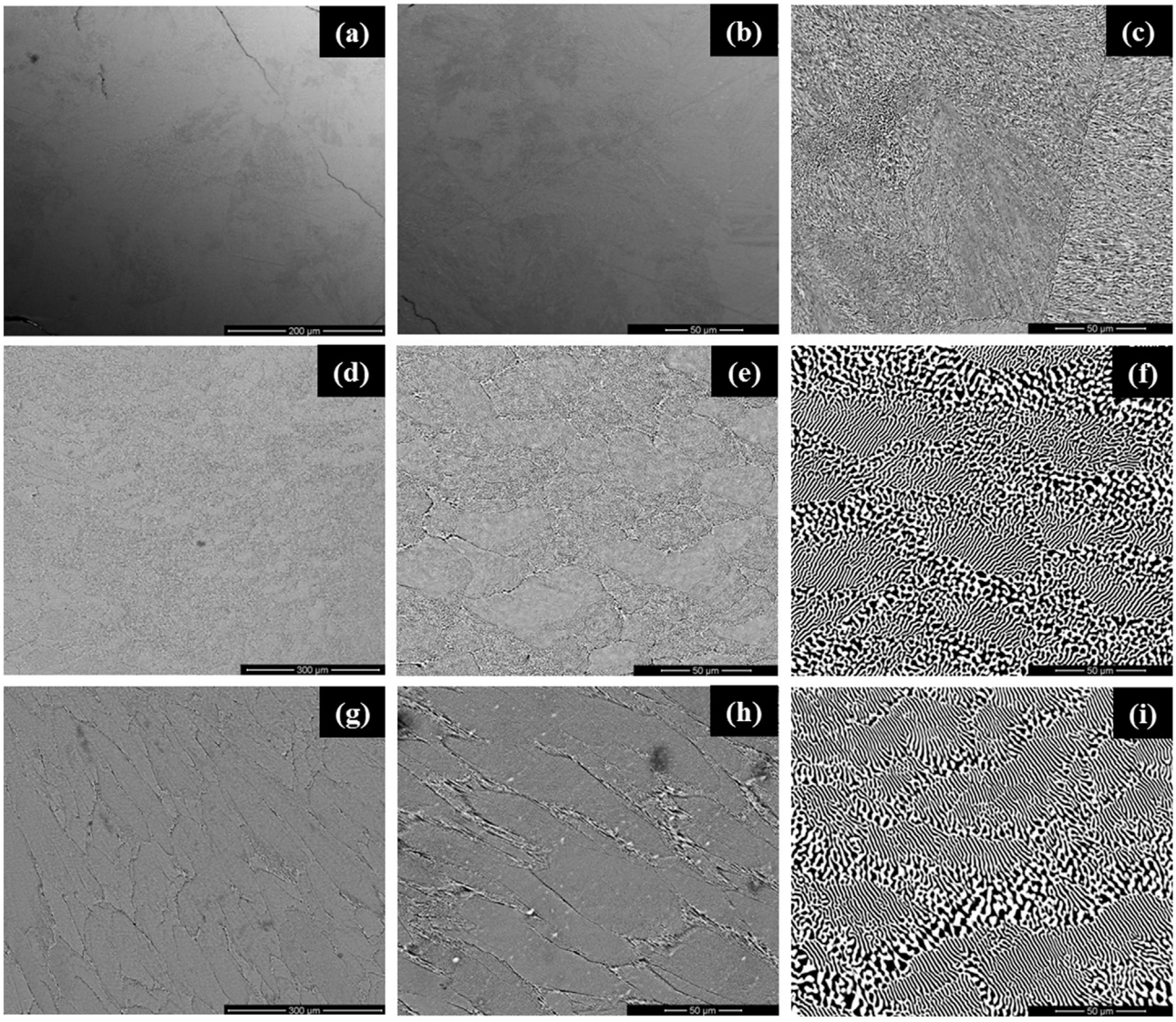

Fig. 3. SEM images of $Mg_{71}Zn_{28.9}Al_{0.1}$ (a, b and c), $Mg_{70}Zn_{24.9}Al_{5.1}$ (d, e and f) and $Mg_{70}Zn_{24.4}Al_{5.6}$ (g, h and i) alloys. In the first column (a, d and g), low magnification (× 400) images of the alloys cooled at 10 °C/min rate are showed. In the second (b, e and h) and third columns (c, f and i), high magnification (× 1200) images of samples cooled at 10 °C/min and 0.1 °C/min rate are showed, respectively.

the $Mg_{21}Zn_{25}$ phase causes some deformation in its structure and gets bigger its lattice parameters. Similar extension solubility results were observed in previous study of Sn-Bi alloy system with an extension of solid solubility up to 35 at.% Bi content [45,46]. Overall, the SEM-EDX results are in agreement with the XRD analysis and confirm the presence of only two phases $Mg_{21}Zn_{25}$ and Mg in the studied materials.

3.2. Thermophysical characterization

3.2.1. Density

The determination of the density (ρ) is an important data not only to determine compaction of obtained samples but also to calculate the storage energy density of TES materials. Two techniques are used to determine the density of the materials:

Table 3
Results of the phase compositions and their proportions for $Mg_{71}Zn_{28.9}Al_{0.1}$, $Mg_{70}Zn_{24.9}Al_{5.1}$ and $Mg_{70}Zn_{24.4}Al_{5.6}$ alloys.

Material	Composition of expected phases	Proportion of expected phases (at.%)	Composition of observed phases by EDX analysis	Proportion of observed phases (at.%)
$Mg_{71}Zn_{28.9}Al_{0.1}$	Mg	46	$Mg_{0.95}Zn_{0.04}Al_{0.01}$	43
	$Mg_{21}Zn_{25}$	54	$Mg_{24.4}Zn_{21.6}$	57
$Mg_{70}Zn_{24.9}Al_{5.1}$	Mg	46	$Mg_{0.91}Zn_{0.08}Al_{0.01}$	52
	$Mg_{21}Zn_{25}$	36	$Mg_{21.6}Zn_{20.7}Al_{3.7}$	48
	$Mg_{32}(Al, Zn)_{49}$	18	–	
$Mg_{70}Zn_{24.4}Al_{5.6}$	Mg	46	$Mg_{0.89}Zn_{0.09}Al_{0.02}$	56
	$Mg_{21}Zn_{25}$	32	$Mg_{21.2}Zn_{20.2}Al_{4.6}$	44
	$Mg_{32}(Al, Zn)_{49}$	22	–	

Table 4
Theoretical, calculated and experimental density values at room temperature of $Mg_{71}Zn_{28.9}Al_{0.1}$, $Mg_{70}Zn_{24.9}Al_{5.1}$ and $Mg_{70}Zn_{24.4}Al_{5.6}$ alloys.

Material	Density (g/cm^3)		
	Theoretical	Experimental (pycnometer)	Experimental (archimedes method)
$Mg_{71}Zn_{28.9}Al_{0.1}$	3.09	3.00	2.89
$Mg_{70}Zn_{24.9}Al_{5.1}$	3.02	2.82	2.76
$Mg_{70}Zn_{24.4}Al_{5.6}$	3.01	2.79	2.73

Archimedes technique and helium pycnometer (AccuPyc-II 1340 from Micromeritics), which is an accurate technique for measuring the density of alloys [47]. Table 4 summarizes different density values for each alloy, the theoretical value calculated from the pure expected phases obtained from the ternary phase diagram, and the experimental values obtained by helium pycnometer and Archimedes techniques measurements. As it can be observed, the density decreases with the decrease of Zn proportion in the alloys. This effect is due to the higher Zn density compared to Mg and Al ones. In the investigated alloys, the experimental density values measured by the Archimedes technique are smaller than the ones obtained by helium pycnometer. The deviation is less than 4% and corresponds to the open pores in the materials. The experimental helium pycnometer densities are smaller than the calculated ones and the difference is less than 3% which corresponds to the closed pores in the samples. So, this slight reduction in density values confirms the compactness of the materials. The total amounts of the open and close pores are less than 6%.

3.2.2. Calorimetric analysis

Fig. 4 shows the heating and cooling curves of DSC measurements for $Mg_{71}Zn_{28.9}Al_{0.1}$, $Mg_{70}Zn_{24.9}Al_{5.1}$ and $Mg_{70}Zn_{24.4}Al_{5.6}$ alloys. The three alloys show similar behaviour with similar melting and solidification temperatures and enthalpies. Hysteresis values between 8 °C and 11 °C are observed. However, the slight compositional differences between the investigated alloys lead to different phase transition mechanisms.

Fig. 4 (a) shows the heating and cooling curves of $Mg_{71}Zn_{28.9}Al_{0.1}$ quasi-peritectic alloy. Its behaviour is similar to the binary eutectic $Mg_{72}Zn_{28}$ alloy due to their close compositions. On the heating run, two partially overlapped transformation processes are found. The first peak at 335 °C corresponds to the eutectoid solid-solid phase transformation $Mg_{0.95}Zn_{0.04}Al_{0.01} + Mg_{24.4}Zn_{21.6} \rightarrow (Mg_{51}Zn_{20})$. The second one at 343 °C is associated to the solid-liquid phase transition $(Mg_{51}Zn_{20}) + Mg_{24.4}Zn_{21.6} \rightarrow L$. Due to the overlapping between both transformation processes it is difficult to obtain accurate individual transformation enthalpy values. However, the overall enthalpy associated to both transitions is 153 J/g. On the cooling run, both transformation processes are totally overlapped and a single calorimetric peak is obtained at 332 °C with a transition enthalpy of 154 J/g. Fig. 4 (b) displays the heating and cooling curves of $Mg_{70}Zn_{24.9}Al_{5.1}$ eutectic alloy. On the heating $Mg_{0.91}Zn_{0.08}Al_{0.01} + Mg_{21.6}Zn_{20.7}Al_{3.7} \leftrightarrow L$ eutectic phase transition occurs at 340 °C with an enthalpy value of 157 J/g. On the cooling run the solidification process occurs at 330 °C with an enthalpy of 157 J/g. Fig. 4 (c) displays the heating and cooling curves of $Mg_{70}Zn_{24.4}Al_{5.6}$ quasi-peritectic alloy. According to phase diagram, two transformation processes are expected; the first one corresponds to eutectic phase transition and the second one, due to quasi-peritectic nature of the alloy, is associated to the melting of primary crystal. As it can be seen from the curve, only a single large peak is obtained at 341 °C and is related to the overlapping of both transformations with an overall enthalpy of 157 J/g. During the cooling run two partially overlapped transformation processes are found. A first peak at 359 °C corresponds to solidification of the mentioned primary crystals and the second one corresponds to $L \rightarrow Mg_{0.89}Zn_{0.09}Al_{0.02} + Mg_{21.2}Zn_{20.2}Al_{4.6}$ eutectic phase transition at 333 °C.

It has to be noted that the three alloys show stable phase transitions unlike observed metastable nature in the $Mg_{72}Zn_{28}$ binary eutectic alloy [26]. On the other hand, the absence of $Mg_{32}(Al, Zn)_{49}$ intermetallic compound does not affect the phase transition behaviour of the $Mg_{70}Zn_{24.9}Al_{5.1}$ eutectic alloy, which shows a single and narrow peak in phase transition process, which ensures the eutectic and homogeneous nature of alloy sample. In contrast, the other two investigated alloys show the contribution of secondary peaks due to their chemical composition. In this way, a eutectoid reaction in $Mg_{71}Zn_{28.9}Al_{0.1}$ quasi-peritectic composition and primary crystals melting and solidification processes in $Mg_{70}Zn_{24.4}Al_{5.6}$ quasi-peritectic alloy have been observed.

The observed behaviours of DSC curves of the investigated alloys are in agreement with the expected reactions sequences and also with the theoretical and experimental melting temperatures and transition enthalpies values reported by several authors [48–50].

3.2.3. Specific heat

The specific heat (C_p) of the alloys has been measured by means of the modulated DSC method from −80 °C to 200 °C for $Mg_{71}Zn_{28.9}Al_{0.1}$ and $Mg_{70}Zn_{24.4}Al_{5.6}$ alloys. The specific heat data of

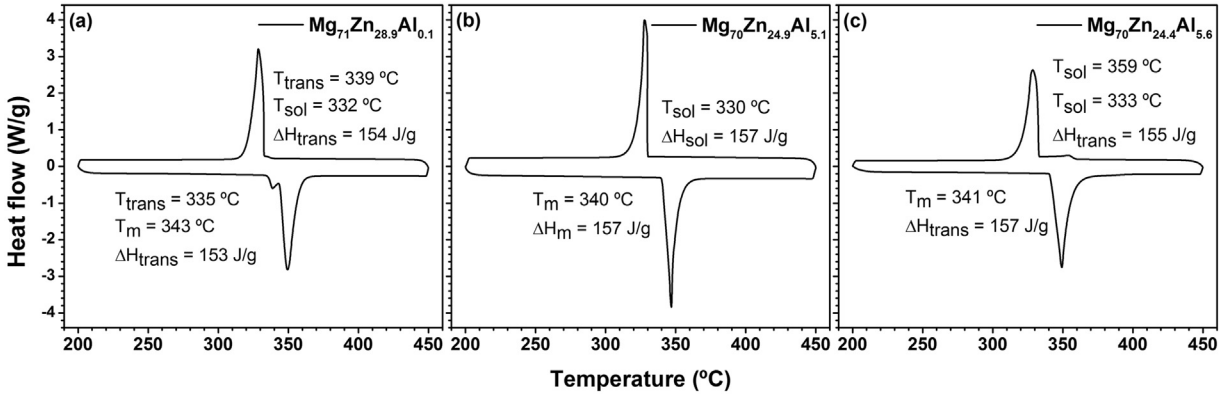

Fig. 4. Melting and solidification temperatures and enthalpies obtained from DSC results at 10 °C/min heating/cooling rates. In (a) the values for $Mg_{71}Zn_{28.9}Al_{0.1}$ quasi-peritectic alloy, in (b) the values for $Mg_{70}Zn_{24.9}Al_{5.1}$ eutectic alloy and (c) the values for $Mg_{70}Zn_{24.4}Al_{5.6}$ quasi-peritectic alloy.

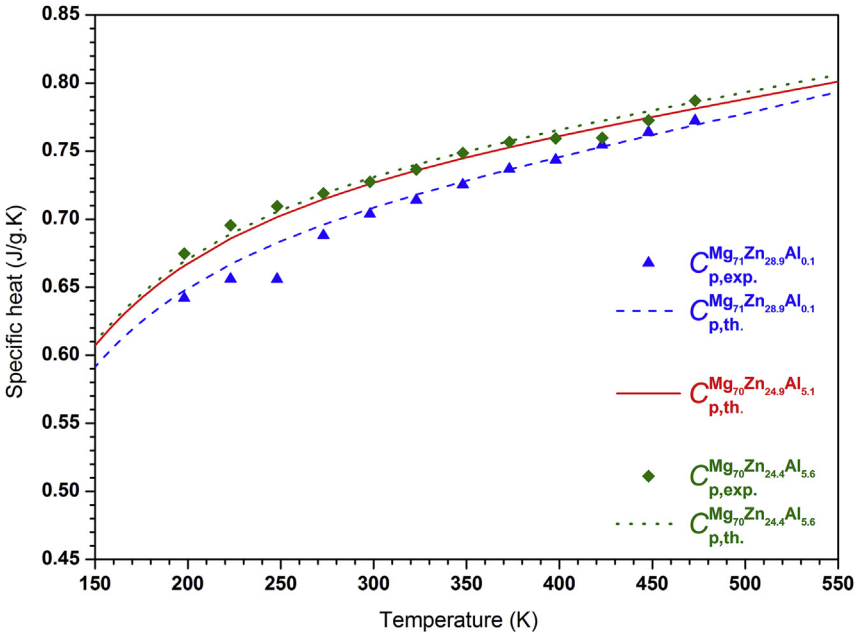

Fig. 5. The experimental and calculated C_p data for (blue) $Mg_{71}Zn_{28.9}Al_{0.1}$ and (green) $Mg_{70}Zn_{24.4}Al_{5.6}$ alloys. The calculated C_p data for (red) $Mg_{70}Zn_{24.9}Al_{5.1}$ alloy. (For interpretation of the references to colour in this figure legend, the reader is referred to the web version of this article.)

$Mg_{70}Zn_{24.4}Al_{5.6}$ alloy are not presented due to their similarity of Cp values of $Mg_{70}Zn_{24.8}Al_{5.1}$. As it was explained recently in Ref. [27] the C_p of metal alloys can be calculated in the complete temperature range through a theoretical approach. This thermodynamic calculation has been used to determine the C_p of the three investigated alloys. The experimental and calculated data show good agreements as can be clearly observed in Fig. 5. Then, three alloys show similar C_p values with a difference around 1–4% at 300 °C. On the other hand, $Mg_{71}Zn_{28.9}Al_{0.1}$ alloy presents the lower C_p values due to its lower content of Al. The obtained values at 25 °C is around 0.70 J/g·K, 0.72 J/g K and 0.73 J/g K for $Mg_{71}Zn_{28.9}Al_{0.1}$, $Mg_{70}Zn_{24.9}Al_{5.1}$ and $Mg_{70}Zn_{24.4}Al_{5.6}$ alloys, respectively.

3.2.4. Thermal diffusivity and thermal conductivity

The high thermal conductivity (λ) of metals and alloys is the main advantage when compared with current heat storage materials, such as molten salts. Fig. 6 shows the thermal diffusivity (α) curves of the three investigated materials obtained by means of the laser flash technique. The measurements are obtained in the temperature range from 50 °C to 400 °C covering the solid and liquid phases. The obtained thermal diffusivities at room temperature of $Mg_{71}Zn_{28.9}Al_{0.1}$, $Mg_{70}Zn_{24.9}Al_{5.1}$ and $Mg_{70}Zn_{24.4}Al_{5.6}$ materials are 26.2 mm^2/s, 22.5 mm^2/s and 20.4 mm^2/s, respectively. In the solid phase range, up to around 320 °C, the curves are approximately constant and then, after the melting process, the measured values

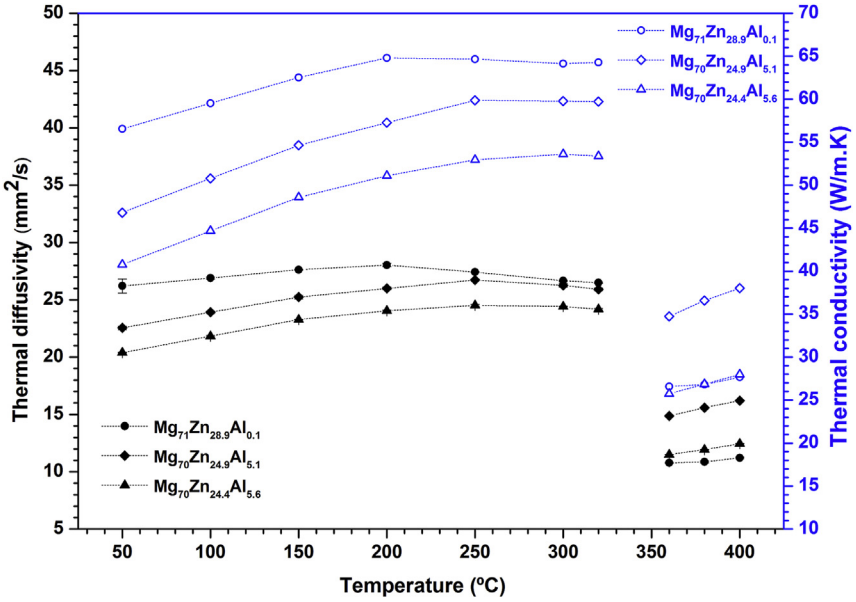

Fig. 6. Thermal diffusivity and conductivity of (circle) $Mg_{71}Zn_{28.9}Al_{0.1}$, (diamond) $Mg_{70}Zn_{24.9}Al_{5.1}$ and (triangle) $Mg_{70}Zn_{24.4}Al_{5.6}$ alloy compositions. The thermal diffusivity is indicated by open symbols and the thermal conductivity by solid symbols. Dotted line is a guide for the eyes.

decrease around the half, 11.0 mm^2/s, 14.9 mm^2/s and 11.4 mm^2/s at 350 °C for $Mg_{71}Zn_{28.9}Al_{0.1}$, $Mg_{70}Zn_{24.9}Al_{5.1}$ and $Mg_{70}Zn_{24.4}Al_{5.6}$ alloys, respectively.

According to Equation (1), the thermal conductivity (λ) was calculated in a temperature range from 50 °C to 400 °C using the following parameters: (i) The experimental thermal diffusivity (ii) the density, which has been approximated to a constant value equal to the one measured at room temperature (iii) the calculated C_p values due to the lack of experimental data in the complete temperature range. Fig. 6 shows the obtained λ values for the investigated alloys. The thermal conductivities at 50 °C are 56.5 W/m K, 46.8 W/m K and 40.8 W/m K for the $Mg_{71}Zn_{28.9}Al_{0.1}$, $Mg_{70}Zn_{24.9}Al_{5.1}$ and $Mg_{70}Zn_{24.4}Al_{5.6}$ alloys, respectively. Similar behaviour to the thermal diffusivity curves is observed due to the quasi linear behaviour of the specific heat and the constant value of the density in this range of temperature. Thereby, the thermal conductivity curves are approximately constant in the solid phase and decrease up to half in liquid phase. However, the three investigated alloys present high thermal conductivity values, being the lowest value in liquid phase 26.6 W/m K, 34.7 W/m K and 25.7 W/m K for $Mg_{71}Zn_{28.9}Al_{0.1}$, $Mg_{70}Zn_{24.9}Al_{5.1}$ and $Mg_{70}Zn_{24.4}Al_{5.6}$ alloys, respectively.

The obtained thermal conductivity values for the three alloys are smaller than the obtained for the $Mg_{72}Zn_{28}$ binary eutectic alloy [26]. This result is due to the periodicity reduction of unit cells of Mg and $Mg_{21}Zn_{25}$ phases due to Al presence in them, As an example, the $Mg_{70}Zn_{24.9}Al_{5.1}$ eutectic alloy with around 5 at.% of the Al content shows a value of thermal conductivity 30% lower than the obtained for the $Mg_{72}Zn_{28}$ alloy at 50 °C and the $Mg_{71}Zn_{28.9}Al_{0.1}$ alloy with a small amount of 0.1 at.% Al shows 15.6% lower thermal conductivity than the eutectic Mg-Zn binary alloy.

4. Conclusions

In this work, $Mg_{71}Zn_{28.9}Al_{0.1}$ (quasi-peritectic), $Mg_{70}Zn_{24.9}Al_{5.1}$ (eutectic) and $Mg_{70}Zn_{24.4}Al_{5.6}$ (quasi-peritectic) alloys have been selected as potential PCMs. The structural and thermophysical characterization of the selected alloys confirms that the three compositions are suitable to be used as high thermal conductivity phase change materials for thermal energy storage applications. The studied metal alloys have shown high structural stabilities in comparison to the binary eutectic $Mg_{72}Zn_{28}$ metal alloy which has shown a random formation of stable and metastable phases. In this work, independently of the cooling rate only the stable phase compositions, even in $Mg_{71}Zn_{28.9}Al_{0.1}$ metal alloy where a small amount 0.1 at.% of Al content is present, have been established at room temperature. The experimental values of the thermophysical properties obtained for $Mg_{71}Zn_{28.9}Al_{0.1}$, $Mg_{70}Zn_{24.9}Al_{5.1}$ and $Mg_{70}Zn_{24.4}Al_{5.6}$ alloys are similar. A large difference was obtained for the thermal diffusivity and conductivity properties. In this regard, a small variation of around 5% in the Al content in the alloy lead to a difference of around 29% in the measured thermal conductivity. Their thermal conductivity values are also smaller than the obtained for the $Mg_{72}Zn_{28}$ binary eutectic alloy. These thermal conductivity reductions are due to Al presence in Mg and $Mg_{21}Zn_{25}$ phases, which reduces the periodicity of their unit cells and as consequence the mean free path of electrons in the crystalline structures of phases. However, the obtained thermal conductivity values for the studied alloys are still high, being the lower value around 26 W/m·K in liquid phase. The high thermal conductivity of the investigated metallic PCMs will allow the design and construction of TES devices with extremely fast charging/discharging rates.

In general, this investigation has shown the high potential of Mg-Zn-Al ternary system in thermal energy storage area. Within the studied compositions, the $Mg_{70}Zn_{24.9}Al_{5.1}$ eutectic alloy could be the best candidate for this kind of application due to its eutectic nature which will display better its long term thermal stability. However, in order to highlight this point, further experimental works are on-going in our laboratory to study the long-term stability of these materials, as well as, the possible oxidation during long term thermal cycling. So, some preliminary results have been published in Refs. [51], where $Mg_{70}Zn_{24.9}Al_{5.1}$ eutectic alloy has shown very good stability after 700 thermal cycles.

Acknowledgements

The authors would like to thank the Department of Industry, Innovation, Commerce and Tourism of the Basque Government for funding the ETORTEK CIC Energigune-2011 and ETORTEK CIC Energigune-2014 research programs. The authors would also like to thank Naira Soguero and Anabel Pérez-Checa for their technical support.

References

[1] A. Arteconi, N.J. Hewitt, F. Polonara, State of the art of thermal storage for demand-side management, Appl. Energy 93 (2012) 371–389.
[2] Y. Jian, Q. Falcoz, P. Neveu, F. Bai, Y. Wanga, Z. Wang, Design and optimization of solid thermal energy storage modules for solar thermal power plant applications, Appl. Energy 139 (2015) 30–42.
[3] K. Nithyanandam, R. Pitchumani, Cost and performance analysis of concentrating solar power systems with integrated latent thermal energy storage, Energy 64 (2014) 793–810.
[4] V. Gnaneswar Gude, Energy storage for desalination processes powered by renewable energy and waste heat sources, Appl. Energy 137 (2015) 877–898.
[5] V. Gadhamshetty, V.G. Gude, N. Nirmalakhandan, Thermal energy storage system for energy conservation and water desalination in power plants, Energy 66 (2014) 938e949.
[6] N.R. Jankowski, F.P. McCluskey, A review of phase change materials for vehicle component thermal buffering, Appl. Energy 113 (2014) 1525–1561.
[7] T. Bauer, N. Pfleger, N. Breidenbach, M. Eck, D. Laing, S. Kaesche, Material aspects of solar salt for sensible heat storage, Appl. Energy 111 (2013) 1114–1119.
[8] A.I. Fernández, M. Martínez, M. Segarra, I. Martorell, L.F. Cabeza, Selection of materials with potential in sensible thermal energy storage, Sol. Energy Mater. Sol. Cells 94 (2010) 1723–1729.
[9] R. Domanski, G. Fellah, "Thermoeconomic analysis of sensible heat, thermal energy storage systems", Appl. Therm. Eng. 18 (1998) 693–704.
[10] T. Wang, D. Mantha, R.G. Reddy, "Novel low melting point quaternary eutectic system for solar thermal energy storage", Appl. Energy 102 (2013) 1422–1429.
[11] F. Roget, C. Favotto, J. Rogez, Study of the KNO_3–$LiNO_3$ and KNO_3–$NaNO_3$–$LiNO_3$ eutectics as phase change materials for thermal storage in a low-temperature solar power plant, Sol. Energy 95 (2013) 155–169.
[12] M.M. Kenisarin, Thermophysical properties of some organic phase change materials for latent heat storage. A review, Sol. Energy 107 (2014) 553–575.
[13] M. Liu, W. Saman, F. Bruno, Review on storage materials and thermal performance enhancement techniques for high temperature phase change thermal storage systems, Renew. Sustain. Energy Rev. 16 (4) (2012) 2118–2132.
[14] Y. Li, Y. Zhang, M. Li, D. Zhang, Testing method of phase change temperature and heat of inorganic high temperature phase change materials, Exp. Therm. Fluid Sci. 44 (2013) 697–707.
[15] D. Laing, T. Bauer, D. Lehmann, C. Bahl, Development of a thermal energy storage system for parabolic trough power plants with direct steam, J. Sol. Energy Eng. 132 (2010), 021011.1–021011.8.
[16] B. Cárdenas, N. León, High temperature latent heat thermal energy storage: phase change materials, design considerations and performance enhancement techniques, Renew. Sustain. Energy Rev. 27 (2013) 724–737.
[17] S. Jegadheeswaran, S.D. Pohekar, Performance enhancement in latent heat thermal storage system: a review, Renew. Sustain. Energy Rev. 13 (2009) 2225–2244.
[18] C.E. Birchenall, A.F. Reichman, Heat storage in eutectic alloys, Metall. Trans. phys. Metall. Mater. Sci. 11 (1980) 1415–1420.
[19] C.E. Birchenall, Heat Storage in Alloy Transformations, NASA, 1980. CR-159787.
[20] D. Farkas, C.E. Birchenall, New eutectic alloys and their heats of transformation, Metall. Transform. A 16 (1985) 323–328.
[21] H. Sugo, E. Kisi, D. Cuskelly, Miscibility gap alloy with inverse microstructure and high thermal conductivity for high energy density thermal storage applications, Appl. Therm. Eng. 51 (2013) 1345–1350.
[22] J.Q. Sun, R.Y. Zhang, Z.P. Liu, G.H. Lu, Thermal reliability test of Al-34%Mg-6%

Zn alloy as latent heat storage material and corrosion of metal with respect to thermal cycling, Energy Convers. Manag. 48 (2) (2007) 619–624.
[23] D. Fang, Z. Sun, Y. Li, X. Cheng, Preparation, microstructure and thermal properties of Mg-Bi alloys as phase change materials for thermal energy storage, Appl. Therm. Eng. 92 (2016) 187–193.
[24] R. Adinberg, D. Zvegilsky, M. Epstein, Heat transfer efficient thermal energy storage for steam generation, Energy Convers. Manag. 51 (1) (2010) 9–15.
[25] X. Wang, J. Liu, Y. Zhang, H. Di, Y. Jiang, Experimental research on a kind of novel high temperature phase change storage heater, Energy Convers. Manag. 47 (2006) 2211–2222.
[26] P. Blanco-Rodríguez, J. Rodríguez-Aseguinolaza, E. Risueño, A. Faik, M. Tello, S. Doppiu, Corrigendum to :Thermophysical characterization of Mg-51%Zn eutectic metal alloy: a phase change material for thermal energy storage in direct steam generation applications, Energy 75 (2014) 630.
[27] J. Rodríguez-Aseguinolaza, P. Blanco-Rodríguez, E. Risueño, M.J. Tello, S. Doppiu, Thermodynamic study of the eutectic Mg49–Zn51 alloy used for thermal energy storage, J. Therm. Anal. Calorim. 117 (2014) 93–99.
[28] FactSage, http://www.crct.polymtl.ca/factsage/fs_polythermal_proj.php.
[29] T. Roisnel, J. Rodríguez-Carvajal, WinPLOTR: a Windows tool for powder diffraction patterns analysis, Mater. Sci. Forum 378 (2000) 118–123. Proceedings of the Seventh European Powder Diffraction Conference (EPDIC 7).
[30] J. Rodriguez-Carvajal, T. Roisnel, FullProf.98 and WinPLOTR new windows 99/NT applications for diffraction, Comm. For Powder Diffr. Int. Union Crystallogr. 20 (1998) 35–36.
[31] R.L. Danley, New modulated DSC measurement technique, Thermochim. Acta 402 (2003) 91–98.
[32] J. Blumm, A. Lindemann, S. Min, Thermal characterization of liquids and pastes using the flash technique, Thermochim. Acta 455 (2007) 26–29.
[33] S. Min, J. Blumm, A. Lindemann, A new laser flash system for measurement of the thermophysical properties, Thermochim. Acta 455 (2007) 46–49.
[34] R. Cêrný, G. Renaudin, The intermetallic compound $Mg_{21}Zn_{25}$, Acta Crystallogr. Sect. C 58 (2002) 154–155.
[35] M.E. Straumanis, The precision determination of lattice constants by the powder and rotating crystal methods and applications, J. Appl. Phys. 20 (1949) 726–734.
[36] H. Liang, S.-L. Chen, Y.A. Chang, A thermodynamic description of the Al-Mg-Zn system, Metall. Mater. Trans. 28 (1997) 1725–1734.
[37] G. Bergman, J.L.T. Waugh, L. Pauling, The crystal structure of the metallic phase Mg_{32} (Al, Zn)$_{49}$, Acta Crystalogr. 10 (1957) 254–259.
[38] W. Sun, F.J. Lincoln, K. Sugiyama, K. Hiraga, Structure refinement of (Al, Zn)$_{49}Mg_{32}$-type phases by single-crystal X-ray diffraction, Mater. Sci. Eng. 294–296 (2000) 327–330.
[39] A. Smontara, I. Smiljanića, A. Bilušića, Z. Jagličić, M. Klanjšek, S. Roitsch, J. Dolinšek, M. Feuerbacher, Electrical, magnetic, thermal and thermoelectric properties of the “Bergman phase” Mg32 (Al, Zn)49 Complex Metallic Alloy, J. Alloys Compd. 430 (2007) 29–38.
[40] Y.P. Ren, G.W. Qin, W.L. Pei, S. Li, Y. Guo, H.D. Zhao, Phase equilibria of Mg-rich corner in Mg-Zn-Al ternary system at 300 °C, Transactions Nonferrous Metals Soc. China 22 (2012) 241–245.
[41] D.G. McCartney, J.D. Hunt, R.M. Jordan, The structure expected in a simple ternary eutectic system: Part I. Theory, Metall. Trans. A 11 (1980) 1243–1249.
[42] D.G. McCartney, J.D. Hunt, R.M. Jordan, The structure expected in a simple ternary eutectic system: Part II. The Al-Ag-Cu ternary System, Metall. Trans. A 11 (1980) 1251–1257.
[43] C. Morando, O. Garbellini, H. Palacio, Estructuras de solidificación esperadas en sistemas eutécticos ternarios simples, An. AFA 17 (2005) 234–239.
[44] Y.P. Ren, G.W. Qin, W.L. Pei, Y. Guo, H.D. Zhao, H.X. Li, M. Jiang, S.M. Hao, The α-Mg solvus and isothermal section of Mg-rich corner in the Mg–Zn–Al ternary system at 320 °C, J. Alloys Compd. 481 (2009) 176–181.
[45] R.H. Kane, B.C. Giessen, N.J. Grant, New metastable phases in binary tin alloy systems, Acta Metall. 14 (5) (1966) 605–609.
[46] J.H. Perepezcko, D.H. Rasmussen, I.E. Anderson, C.R. Lopes Jr., in: Proceedings of the International Conference on Solidification, 1, 1977, p. 169.
[47] O. Ast, M. Perez, S. Carlet, Paul alloys density measurements using gas pycnometer: first results, J. Alloys Compd. 444–445 (2007) 226–229.
[48] J.B. Clark, L. Zabdyr, Z. Moser, Phase diagrams of binary magnesium alloys, Alloys Phase Diagr. ASM Int. 3 (1988) 1113.
[49] V. Raghavan, Al-Mg-Zn (Aluminum-Magnesium-Zinc), J. Phase Equilibria Diffus. 28 (2) (2007) 203–208.
[50] P. Liang, T. Tarfa, J.A. Robinson, S. Wagner, P. Ochin, M.G. Harmelin, H.J. Seifert, H.L. Lukas, F. Aldinger, Experimental investigation and thermodynamic calculation of the Al-Mg-Zn System, Thermochim. Acta 314 (1998) 87–110.
[51] E. Risueño, A. Faik, J. Rodríguez-Aseguinolaza, P. Blanco-Rodríguez, A. Gil, M. Tello, B. D'Aguanno, Mg-Zn-Al eutectic alloys as phase change material for latent heat thermal energy storage, Energy Procedia 69 (2015) 1006–1013.